

Article

The Effect of Eutectic Structure on the Creep Properties of Sn-3.0Ag-0.5Cu and Sn-8.0Sb-3.0Ag Solders

Yujin Park ¹, Jung-Hwan Bang ², Chul Min Oh ³, Won Sik Hong ³ and Namhyun Kang ^{1,*} 

¹ Department of Materials Science and Engineering, Pusan National University, Busan 46241, Korea; yujin3584@naver.com

² Micro-Joining Center, Korea Institute of Industrial Technology, Incheon 21999, Korea; nova75@kitech.re.kr

³ Electronic Convergence Materials & Device Research Center, Korea Electronics Technology Institute, Seongnam 13509, Korea; cmoh@keti.re.kr (C.M.O.); wshong@keti.re.kr (W.S.H.)

* Correspondence: nhkang@pusan.ac.kr; Tel.: +82-51-510-3274

Received: 9 November 2017; Accepted: 28 November 2017; Published: 3 December 2017

Abstract: Solder joints are the main weak points of power modules used in harsh environments. For the power module of electric vehicles, the maximum operating temperature of a chip can reach 175 °C under driving conditions. Therefore, it is necessary to study the high-temperature reliability of solder joints. This study investigated the creep properties of Sn-3.0Ag-0.5Cu (SAC305) and Sn-8.0Sb-3.0Ag (SSA8030) solder joints. The creep test was conducted at 175 and 190 °C with the application of 2.45 MPa. The SAC305 solder had superior creep properties to those of SSA8030 solder at 175 °C and at largely the same homologous temperature ($T_H \sim 0.91$ for SAC305 and $T_H \sim 0.92$ for SSA8030). Both solders had primary β -Sn and a eutectic mixture of β -Sn and Ag_3Sn . Compared to SSA8030, the SAC305 solder contained $\sim 10\%$ more eutectic structure and contained Ag_3Sn that was 3 times smaller and more round in shape. Furthermore, the SSA8030 solder precipitated SnSb in an elongated fiber shape (1–50 μm in size) after the creep test. Coarse and elongated Ag_3Sn and SnSb of the SSA8030 solder negatively affected crack propagation in the dislocation creep region and decreased the creep resistance.

Keywords: creep; lead-free solder; Sb solder; Sn-8.0Sb-3.0Ag; solder microstructure

1. Introduction

In order to prevent global warming and other environmental problems, electric and hybrid vehicles are being developed to reduce automobile CO₂ emissions. Development of power modules is essential to obtain high efficiency and current conversion in these vehicles. For power modules made from Si chips, the maximum temperature can increase to 175 °C during operation as they require higher performance and a larger capacity than insulated gate bipolar transistor (IGBT) modules. Therefore, high-temperature reliability needs to be thoroughly evaluated for reliable use of power modules [1–4].

Components for power modules such as semiconductors and terminals are attached using solders. Thermal stress is applied by repeated shrinkage and expansion of solder joints, therefore leading to failure during operation. Because the components for modules in automobiles are used in harsher environments than those of normal electronic components, Pb-rich solders with a high melting point and Pb-containing solders with high reliability have been used for these power modules. However, due to a recent environmental regulation for automobiles, i.e., End-of-Life Vehicle (ELV), the use of Pb-containing solders for electrical components was completely prohibited in the European Union (EU), the European Free Trade Association (EFTA), Japan, Korea, and China. Therefore, studies

on high-temperature Pb-free solder to substitute for conventional Pb-containing solder have been conducted [5–10].

The creep test is essential in evaluating solder joint properties at high temperature. Diffusion and dislocation movement in a material are activated as temperature increases. Therefore, the strength of the material is decreased and eventually deformation is accelerated leading to a fracture although the applied stress is lower than its yield strength. The creep mechanism is classified with respect to homologous temperature (T_H) and stress. Homologous temperature is the ratio between test temperature and melting temperature, and it is an important factor for the creep test because creep strength is sensitive to the test temperature compared to the melting temperature.

Creep mechanism is classified into grain-boundary sliding, dislocation creep, and diffusion creep. Creep deformation induced by grain-boundary sliding occurs when the high stress is applied. On the other hand, creep occurring under low stress is diffusion creep and it can be divided into Coble creep and Nabarro-Herring creep. The creep mechanism most frequently studied is dislocation creep occurring at relatively high temperatures and in moderate stress regions [11–16]. Dislocation creep is caused by movement such as glide or climbing of dislocation and corresponds to Low temperature creep, High Temperature creep, and Power-law break down. The strengthening mechanism of the solder is very important in understanding its high-temperature properties. The strengthening mechanisms that can be used for solidification of solder are solid-solution strengthening and precipitation strengthening. Therefore, the study of solid solution and precipitation is important in understanding dislocation creep because lattice deformation due to solid solution and precipitation interfere with the movement of the dislocation.

There are many studies on Pb-free solders, but very few studies on their creep properties have been reported for Pb-free solders used in high-temperature environments [17]. Recently, researchers have studied nano-indentation requiring a short creep test time [18,19]. However, nano-indentation creep is influenced only by microstructures near the dent area, and complex microstructures such as primary phase, eutectic structure, and precipitation need to be considered for a full understanding of creep properties. Pb-containing solders have a sufficient database of creep properties and are primarily composed of Sn. Pb-free solder also has an Sn-rich composition and the creep mechanism map of Sn–Pb solder has been used for Pb-free solder [20]. This study measured the creep properties of Sn-3.0Ag-0.5Cu (SAC305), the most commonly used solder, and Sn-8.0Sb-3.0Ag (SSA8030), a high melting point solder, and analyzed the microstructure of the joint to understand the creep mechanism.

2. Materials and Methods

2.1. Preparation of Creep Specimen

Figure 1 shows a schematic diagram of the power module used in this the study. Solder joints where Si chips and terminals are attached to direct bonded copper (DBC) are the main cause of failure. The terminal used for the power module was fixed to a plastic case, followed by attachment to the DBC using two types of solder. The terminals were coated with Sn and the surface of the DBC coupons were treated with organic solderability preservative (OSP) such as alkylbenzimidazole and diphenylimidazole. SAC305 and SSA8030 used for the solder have a melting temperature of 217 and 232 °C, respectively. The fixed terminals are vulnerable to stress when the solder solidify for reflow soldering and the assembled parts to vehicles are in operation. This becomes a reason for creep fracture at the operating temperature of 175 °C. Figure 1 shows the creep test with the terminal coupons.

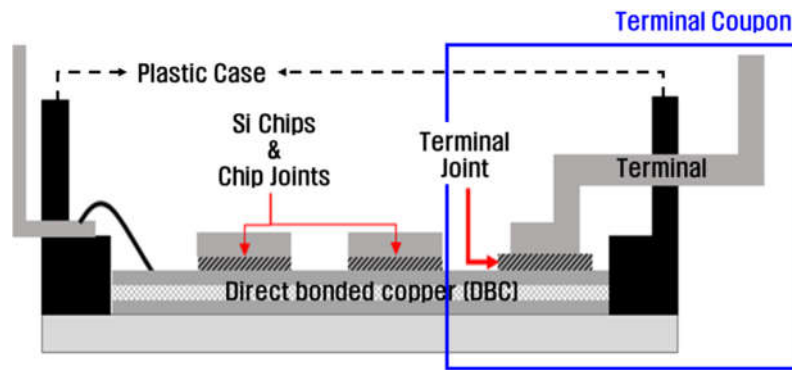


Figure 1. Schematic diagram of power module showing the terminal joint.

2.2. Creep Test

Figure 2 shows a strain measured for the terminal due to expansion and contraction during reflow soldering. A strain gauge was attached to the terminal during terminal soldering to the DBC. The strain of the terminal was measured three times in total, and it showed maximum strains of 1.07×10^{-3} , 7.91×10^{-4} , and 8.14×10^{-4} , respectively. Because the average strain was 8.92×10^{-4} and the length of the terminal (L) was 4 mm, the average-maximum displacement (ΔL) corresponding to the average strain was calculated to be $3.57 \mu\text{m}$ using Equation (1):

$$\text{strain} = \frac{\Delta L(\text{displacement})}{L(\text{length})}. \quad (1)$$

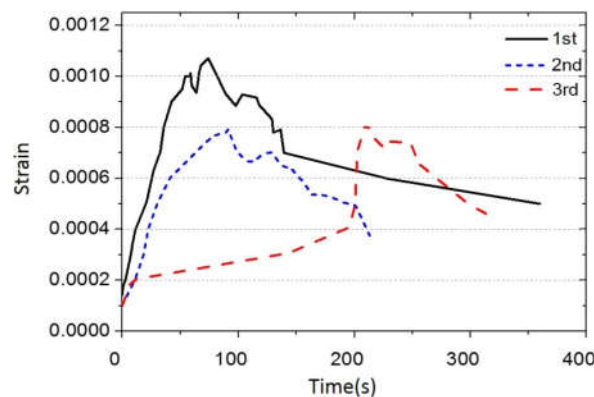


Figure 2. Strain measured for soldering the terminals to the direct bonded copper (DBC).

We applied the calculated displacement (ΔL) to the force–displacement relation obtained through the experiment of the shear stress at the terminal joint, and calculated the stress of the solder joint caused by the displacement. Figure 3 indicates the shear force and displacement behavior measured for the terminal-solder joint. The solid black line of Figure 3 is the shear force and displacement measured for the terminal joint. The red dotted line shows the regression relationship between the displacement and the force in the elastic region. The slope of red dotted line (40.86) shows a different value as compared with the shear modulus of bulk solder (16.60 GPa). The calculated regression equation is as follows:

$$y(\text{force}) = 40.86 \times \Delta L(\text{displacement}) + 1636.8. \quad (2)$$

Substituting the displacement of $3.57 \mu\text{m}$ into Equation (2), the stress was calculated to be 2.18 MPa and the load of 1.7 kg is obtained by multiplying the force with the joining area (8 mm^2). When the stress of 2.18 MPa is applied at $175 \text{ }^\circ\text{C}$, dislocation creep will occur at the SAC305 and SSA8030 terminal

joints. In order to reliably proceed with the creep test in the dislocation creep area, we applied a stress of 2.45 MPa to the terminal using a weight of 2 kg.

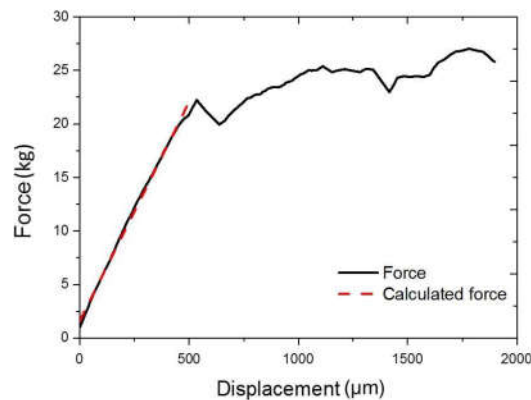


Figure 3. Shear force–displacement behavior measured for terminal-solder joints and the regression line calculated in the elastic region.

The conditions of the creep test such as stress, temperature, and T_H are shown in Table 1. We determined creep failure from the time when the terminal was electrically disconnected completely from the DBC. To observe the failure time, we used a multi-channel multimeter to check electrical resistance every second, and the test was repeated five times in each conditions. We conducted the creep test at maximum operating temperatures of 175 and 190 °C to consider the influence of T_H on creep behavior.

Table 1. Conditions of the creep test.

Solders	SAC305		SSA8030	
Melting temperature	217 °C		234 °C	
Creep test temperature	175 °C	190 °C	175 °C	190 °C
T_H	0.91	0.94	0.88	0.92
Stress	2.45 MPa			

2.3. Microstructure

For microstructural observation, specimens were cold-mounted with conductive copper resin. The mounted specimens were subjected to a final polishing using 0.05 μm colloidal silica. The microstructure was observed using the back-scattered electron (BSE) mode of a field-emission scanning electron microscopy (FE-SEM, TESCAN, Brno, Czech Republic) with no etching. We measured the composition of the phase using energy dispersive spectroscopy (EDS) and field-emission electron probe micro analysis (FE-EPMA, JEOL, Tokyo, Japan). In order to observe the crystal orientation and stress distribution, we applied argon ion milling treatment on the specimens after final polishing, followed by electron back-scattered diffraction (EBSD). The amount and shape of the microstructures were measured from 5 to 10 images, and the average value was calculated using the i-solution DT program (IMT i-solution Inc., TX, USA).

3. Results

3.1. Effect of Solder Composition and Test Temperature on Creep Failure

Figure 4 shows the creep failure time for the SAC305 and SSA8030 solders at 175 and 190 °C. At 175 °C, the failure time of the SAC305 and SSA8030 solder was 207 min and 84 min, respectively. At 190 °C, the failure time of the SAC305 solder was 66 min and that of the SSA8030 solder was 47 min.

The SAC305 solder, compared to the SSA8030 solder, exhibited a better creep property at both 175 and 190 °C. Considering the relative ratio of test temperature with respect to melting temperature, for the same T_H values of 0.91 (175 °C for SAC305) and 0.92 (190 °C for SSA8030), the failure time was recorded to be 207 and 47 min, respectively. Therefore, the creep property of the SAC305 was significantly superior to that of the SSA8030 for the approximately same T_H level.

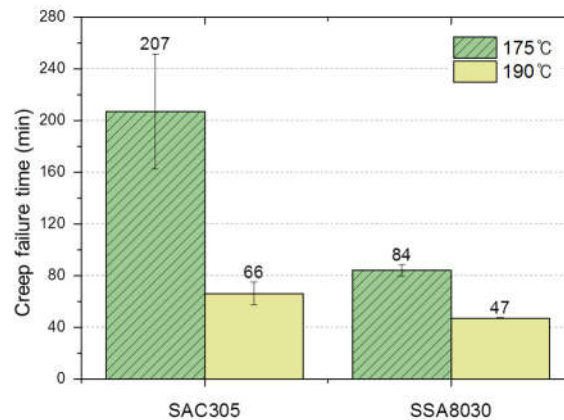


Figure 4. Effects of solders and test temperature on creep failure time. The bars correspond to standard deviations.

Figure 5 shows the fracture surface after the creep test at 175 °C. The SAC305 solder exhibited an elongated dimple fracture parallel to the direction of applied load (Figure 5a). Figure 5b shows the fracture surface at high magnification ($\times 10,000$) for the SAC305 solder joint. We measured a dimple size of approximately 10 μm and noted that Ag_3Sn had precipitated on the dimple surface. For the SSA8030 solder, it was difficult to distinguish the dimple shape clearly at low magnification (Figure 5c) because it is more vulnerable to oxidation than the SAC305 [21]. However, in Figure 5d, dimples approximately 10 μm in size were observed and SnSb and Ag_3Sn were precipitated on the dimple surface. Based on EDS analysis, Ag_3Sn grew in a round shape, as shown in Figure 5b,d. However, SnSb was precipitated in an irregular and sharp shape (Figure 5d) on the SSA8030. Coarse SnSb precipitates of large size ($\sim 50 \mu\text{m}$) and rough surface were also observed as shown in Figure 5c.

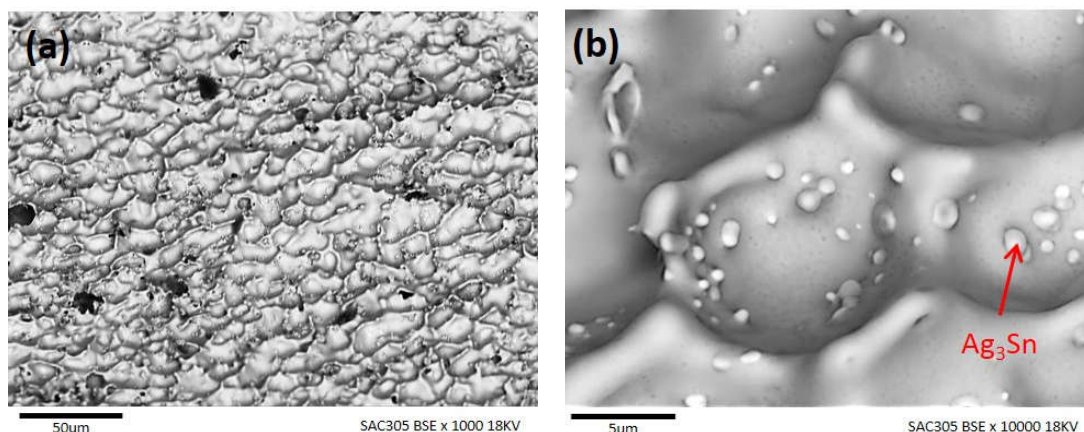


Figure 5. Cont.

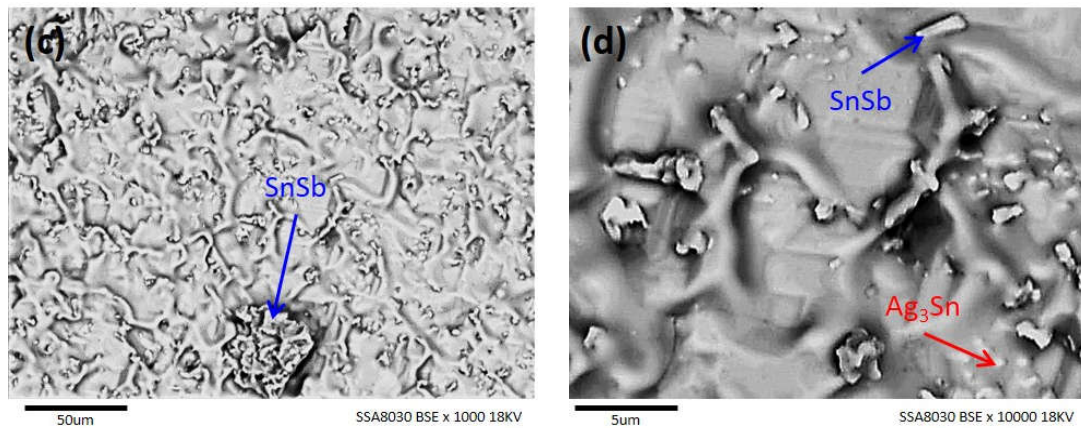


Figure 5. Fracture surface after creep testing at 175 °C: (a,b) SAC305 solder joints; (c,d) SSA8030 solder joints.

3.2. Effect of Solder Composition on Microstructure

Figure 6a,c shows the microstructures in BSE mode before and after the creep experiment of the SAC305 solder joint, respectively, and Figure 6b,d shows those of the SSA8030 solder joint, respectively. The light gray microstructure is the primary β -Sn, the dark gray is the eutectic mixture of β -Sn and Ag_3Sn , and the black is the Cu_6Sn_5 . The SSA8030 and SAC305 solders had the same type of microstructure. The SSA8030 had no Cu content but produced Cu_6Sn_5 by diffusion of Cu from the DBC substrate during reflow soldering. The amount of Cu_6Sn_5 increased after the creep test for the SAC305 and SSA8030 solders (Figure 6c,d). The SSA8030 solder indicated a coarser Cu_6Sn_5 than the SAC305. After the creep test, we measured the area fraction of Cu_6Sn_5 in the SAC305 solder and SSA8030 solder to be 2.0% and 3.9%, respectively. Although the SAC305 solder had less Cu_6Sn_5 than the SSA8030 solder, the SAC305 solder had smaller and uniformly distributed Cu_6Sn_5 . Both of the solders had largely the same width of β -Sn dendrites, and their widths were approximately 12 μm , which was similar to the dimple size ($\sim 10 \mu\text{m}$) of the fracture surface shown in Figure 5b,d. In other words, decohesion occurred at the boundary due to the strength difference between the eutectic region reinforced by Ag_3Sn and the relatively low strength of the β -Sn dendrite region. Finally, a dimple fracture formed by the cavity growth [22]. We also confirmed it by the Ag_3Sn detected on the dimple surface (Figure 5b,d).

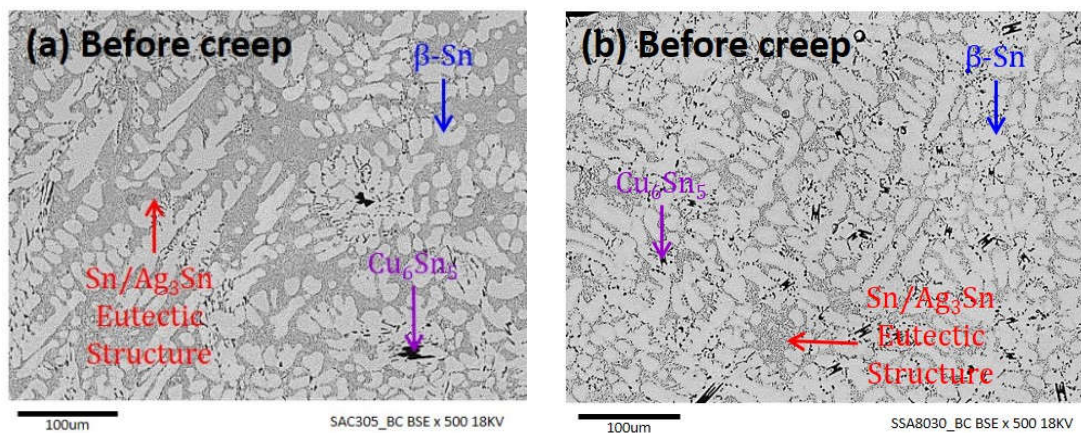


Figure 6. Cont.

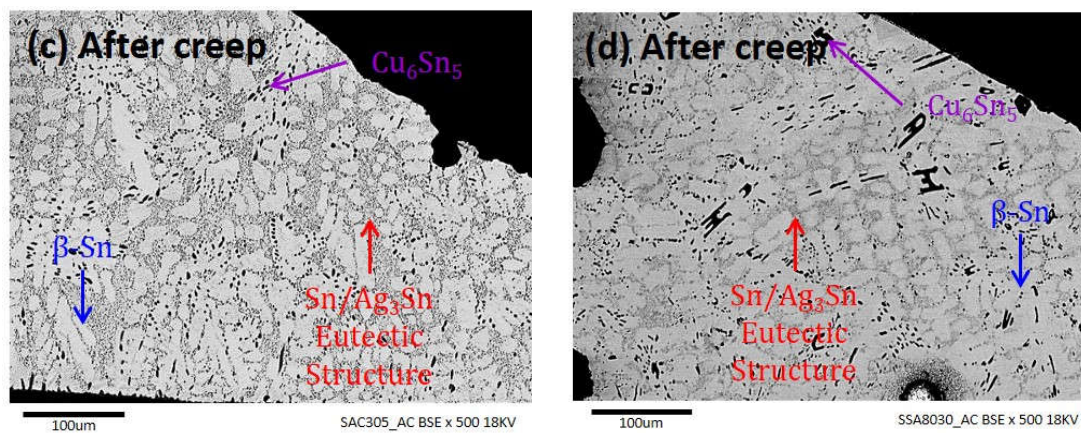


Figure 6. Microstructure before and after the creep test, respectively, for (a,c) SAC305 and (b,d) SSA8030 solders.

Figure 7a shows the EBSD phase map with Sn in red and Cu_6Sn_5 in green. Black dots in the red region were confirmed as Ag_3Sn precipitate using EDS. Figure 7b is the kernel average misorientation (KAM) map that shows the stress field through a variation of the local crystal orientation [23]. We observed a stress field of green and red around the interface where Cu_6Sn_5 and Ag_3Sn formed. Because the stress field prevents the movement of dislocation and plastic deformation, the precipitation of Cu_6Sn_5 and Ag_3Sn is related to the creep strength.

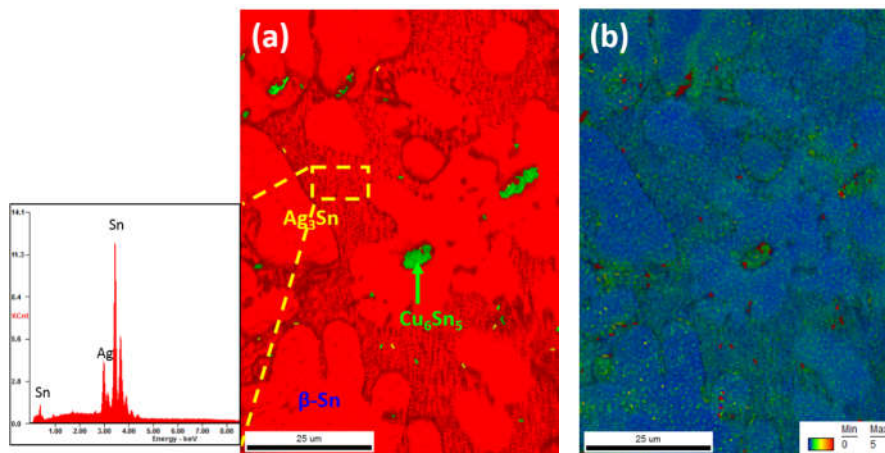


Figure 7. EBSD images of SAC305 before the creep test: (a) inverse pole figure (IPF); (b) kernel average misorientation (KAM).

Unlike Sn-37Pb solders producing a lamella-eutectic structure, Pb-free solders produce dispersed Ag_3Sn with a fibrous form around the primary $\beta\text{-Sn}$ [24,25]. Ag_3Sn is a thermally stable compound because of the limited solubility of Ag in $\beta\text{-Sn}$ [26,27]; therefore, it strengthens the eutectic structure. Ag_3Sn is one of the components in the eutectic mixture for Sn-rich Pb-free solders containing Ag content. Figure 8 shows the amount of eutectic structure for the SAC305 and SSA8030 solders. Before the creep test, the SAC305 had the largest amount of eutectic structure (58.5%). After the creep test, the SAC305 solder contained a larger amount of eutectic structure than the SSA8030 solder. The creep test at 175 °C decreased the amount of eutectic structure for both solders. This is because of the Ostwald Ripening effect in which intermetallic compounds (IMCs) smaller than the critical size are resolved, and they combine with the large IMCs, increasing the size of the IMCs [28].

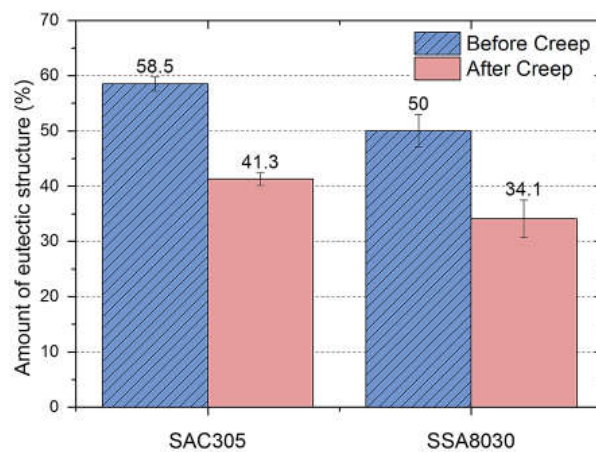


Figure 8. The amount of eutectic microstructure before and after creep testing at 175 °C. The bars correspond to standard deviations.

4. Discussion

Figure 9 shows the eutectic structure observed in detail. The white precipitates are Ag_3Sn and the black are Cu_6Sn_5 . The SAC305 shows Ag_3Sn of smaller size and of a rounder shape than that of the SSA8030. Furthermore, the SSA8030 produced very small SnSb IMCs (dark gray precipitates in Figure 9d) with some large SnSb IMCs after the creep test. For the precipitates of small size and round shape, their strength increases because they reduce the inter back stress formation and the dislocation movement [29]. Therefore, we measured the size and shape of Ag_3Sn quantitatively and it is shown in Table 2. The precipitate size was measured from the long axis of the precipitates, and the roundness (R) was calculated following ISO16112 using Equation (3) as follows [30]:

$$R = \frac{A/l_m^2}{\pi/4} = \frac{A}{A_m}. \quad (3)$$

R is roundness, l_m is the maximum diameter of the precipitate, A_m is an area of the circle whose diameter is l_m , and A is the actual size of the precipitate.

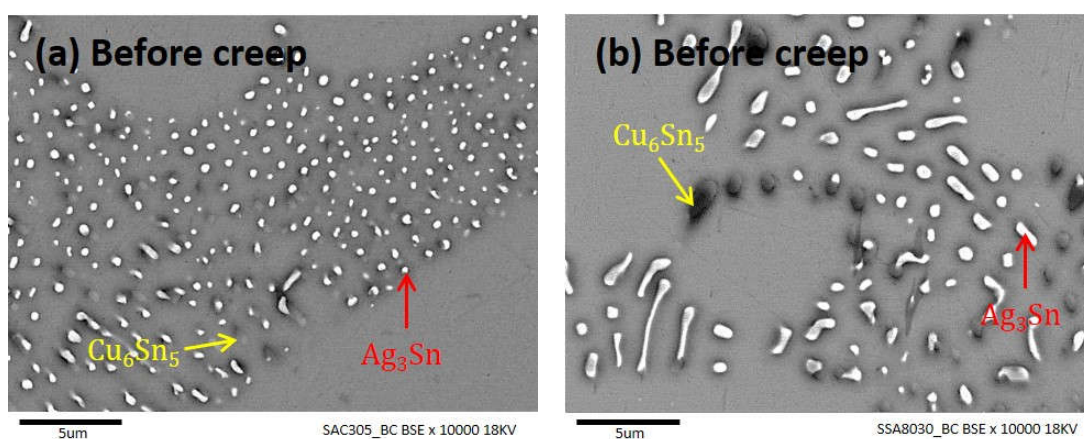


Figure 9. Cont.

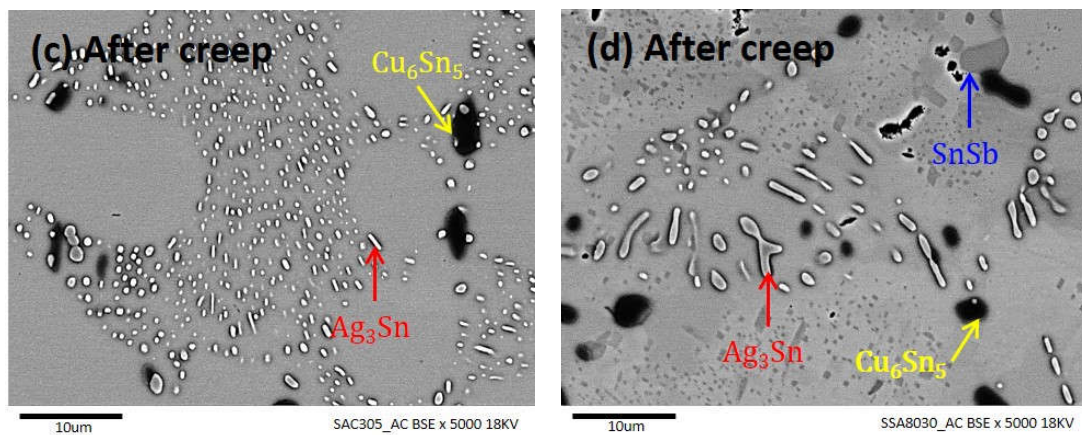


Figure 9. Intermetallic compounds before and after creep testing at 175 °C, respectively, for (a,c) SAC305 and (b,d) SSA8030 solders.

Table 2. Size and shape of Ag₃Sn in eutectic microstructure before and after creep test.

Creep	Solders	Fraction of Ag ₃ Sn (%)	Longer axis of Ag ₃ Sn (µm)	Roundness (R)	Δσ _p (MPa)
Before Creep	SAC305	4.7	0.37	0.88	35.58
	SSA8030	5.7	1.16	0.70	11.08
After Creep	SAC305	4.4	0.48	0.94	24.56
	SSA8030	3.4	1.19	0.79	8.56

The Ag₃Sn in the SAC305 solder had an average size of approximately 0.37 µm and was in a round shape regardless of the creep test. After the creep test at 175 °C, the average size of Ag₃Sn increased to 0.48 µm with no variation in Ag₃Sn fraction. Meanwhile, Ag₃Sn in the SSA8030 solder had an elongated shape and an average size of 1.16 and 1.19 µm, respectively, before and after the creep test. The SSA8030 showed no variation in the average size of Ag₃Sn regardless of the creep test. The SAC305 showed Ag₃Sn that was 3 times smaller and rounder than that of the SSA8030 regardless of the creep test. Moreover, the maximum size of Ag₃Sn in the SSA8030 solder was approximately 7 µm. The coarse Ag₃Sn negatively affects mechanical strength [31]. Fine and abundant Ag₃Sn hinders the movement of dislocation and increases creep properties [32]. In order to analyze quantitatively the mechanical strength variation by precipitate, Equations (4) and (5) were used as follows [33]:

$$\Delta\sigma_p = 5.9 \left(f^{1/2} / x \right) \times [\ln(x/2.5E - 4)] \quad (4)$$

$$x = D \times (2/3)^{1/2}. \quad (5)$$

where f is the volume fraction of the precipitate, x is the mean planar intercept diameter (µm), and D is the mean diameter (µm) of the precipitate. We calculated the strength ($\Delta\sigma_p$) due to the precipitates by substituting the size and amount of Ag₃Sn measured in Figure 9 and Table 2. Because the SAC305 solder had small and round Ag₃Sn, the strength ($\Delta\sigma_p$) due to precipitates was 3 times that of the SSA8030 solder (Table 2). In Equation (4), the volume fraction (f) of the precipitate has a power of 0.5 and it has less influence on the strength than the size factor (x) of the precipitate. Specifically, large and elongated SnSb IMCs were precipitated in the SSA8030 solder after the creep test (Figures 5d and 9d). Therefore, we conducted additional analysis to investigate the effect of the large and elongated SnSb on creep failure.

Figure 10a,b shows the FE-EPMA images of the SSA8030 solder after the creep test at 175 °C. Sn was the most abundant element for β-Sn and the eutectic mixture (Figure 10a). SnSb was distributed irregularly in β-Sn and the eutectic mixture as a red phase, and rich Sb content in β-Sn dendrites was also observed as a light blue phase (Figure 10b). Sb elements were solved in the Sn-rich phase and

produced SnSb during the creep test at 175 °C. Moreover, the creep crack propagated along the coarse SnSb having a size of approximately 50 μm . Figure 10c is the enlarged view of crack propagation through the coarse SnSb IMCs. In the image quality (IQ) map of EBSD, the coarse SnSb was composed of grain boundaries. The crack propagated along the grain boundary of SnSb. Thus, the coarse SnSb precipitates acted as a crack propagation path and decreased the creep properties of the SSA8030 solder.

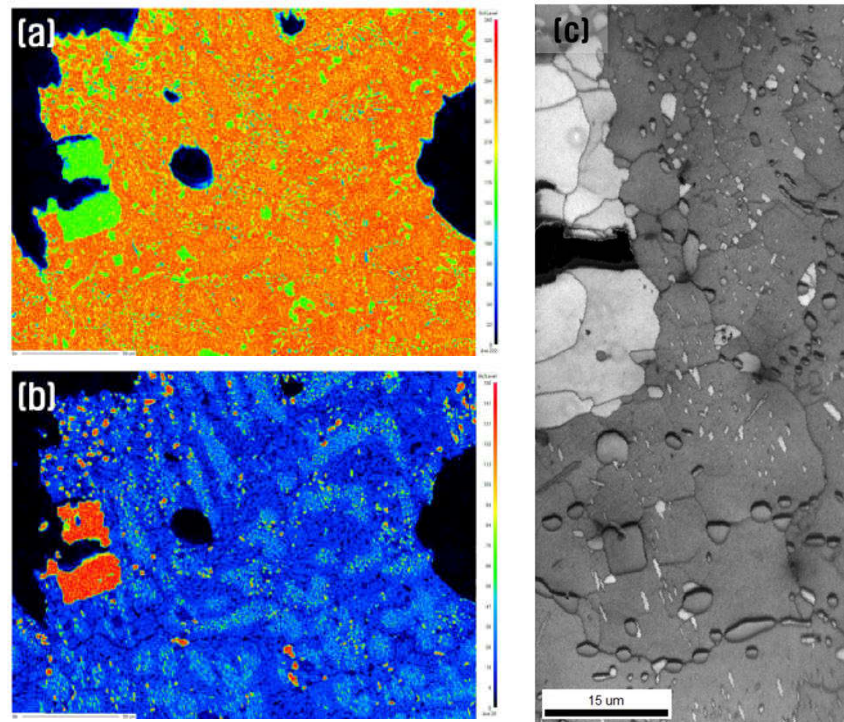


Figure 10. Microstructure of SSA8030 solders after the creep test at 175 °C: (a,b) Sn and Sb mapping using FE-EPMA, respectively; (c) IQ map of EBSD.

The power modules of electric vehicles require a high operating temperature, so the creep properties of terminal-solder joints need to be investigated. However, the size of the terminal-solder joint is so small that the relation of grain boundary and dislocation to the creep properties cannot be observed. For future study, therefore, high-temperature reliability in the scale of bulk solder must be explored so that the creep mechanism of grain-boundary sliding, dislocation creep, and diffusion creep can be understood. Creep properties obtained from bulk solder should be helpful in understanding the real properties of terminal-solder joints.

5. Conclusions

This study investigated the creep properties of the SAC305 and SSA8030 solder joints for the power modules of electric vehicles. The detailed effects of solder composition and microstructure on creep failure time are summarized as follows:

1. During reflow soldering, the terminal joint of the power module corresponded to the dislocation creep region because a stress of 2.18 MPa was applied at the maximum operating temperature of 175 °C.
2. Both solders had primary β -Sn and a eutectic mixture of β -Sn and Ag_3Sn . SAC305 solder contained 58.5% eutectic structure before the creep test after which it decreased to 41.3%. For the SSA8030 solder, the amount of eutectic structure also decreased after the creep test, from 50% to 34.1%. The amount of eutectic structure in the SAC305 solder was larger than in the SSA8030 solder.

3. The SAC305 solder had small and round Ag_3Sn ; therefore, the strength ($\Delta\sigma_p$) due to the precipitates was 3 times greater than that of the SSA8030 solder. The SAC305 solder, compared with the SSA8030 solder, lasted a longer time at 175 °C and at largely the same homologous temperature ($T_H \sim 0.91$ for SAC305 and $T_H \sim 0.92$ for SSA8030).
4. During the creep test, Sb atoms solved in β -Sn precipitated into SnSb in the SSA8030 solder. The coarse SnSb ($\sim 50 \mu\text{m}$) precipitated and became a crack propagation path, therefore decreasing the creep property.

Acknowledgments: This work was supported by the Technology Innovation Program (grant No. 10051318, Development of SiC Automotive OBC Power Module with Environment-Friendly High-Temperature Bonding Materials) funded by the Ministry of Trade, Industry & Energy (MOTIE, Korea) and the National Research Foundation of Korea (NRF) grant funded by the Korea government (MSIT) through GCRC-SOP (grant no. 2011-0030013).

Author Contributions: Y. Park, W.S. Hong and C.M. Oh conceived and designed the experiments; Y. Park performed the experiments; Y. Park and N. Kang analyzed the data; J. Bang contributed reagents/materials/analysis tools; Y. Park and N. Kang wrote the paper.

Conflicts of Interest: The authors declare no conflict of interest.

References

1. Feller, L.; Hartmann, S.; Schneider, D. Lifetime analysis of solder joints in high power IGBT module for increasing the reliability for operation at 150 °C. *Microelectron. Reliab.* **2008**, *48*, 1161–1166. [[CrossRef](#)]
2. Liang, Z. Status and trend of automotive power packaging. *ISPSD* **2012**, *24*, 325–331. [[CrossRef](#)]
3. McCluskey, F.P.; Dash, M.; Wang, Z.; Huff, D. Reliability of high temperature solder alternatives. *Microelectron. Reliab.* **2006**, *46*, 1910–1914. [[CrossRef](#)]
4. Yoon, J.W.; Bang, J.H.; Ko, Y.H.; Yoo, S.H.; Kim, J.K.; Lee, C.W. Power module packaging technology with extended reliability for electric vehicle applications. *J. Microelectron. Packag. Soc.* **2014**, *21*, 1–13. [[CrossRef](#)]
5. Santos, W.L.R.; Brito, C.; Quaresma, J.M.V.; Spinelli, J.E.; Garcia, A. Plate-like cell growth during directional solidification of a Zn-20 wt %Sn high-temperature lead-free solder alloy. *Mater. Sci. Eng. B* **2014**, *182*, 29–36. [[CrossRef](#)]
6. Ji, H.; Qiao, Y.; Li, M. Rapid formation of intermetallic joints through ultrasonic-assisted die bonding with Sn-0.7Cu solder for high temperature packaging application. *Scr. Mater.* **2016**, *110*, 19–23. [[CrossRef](#)]
7. Nahavandi, M.; Hanim, M.A.A.; Ismarrubie, A.N.; Hajalilou, A.; Rohaizuan, R.; Fadzli, M.Z.S. Effects of silver and antimony content in lead-free high-temperature solders of Bi-Ag and Bi-Sb on copper substrate. *J. Electron. Mater.* **2014**, *43*, 579–585. [[CrossRef](#)]
8. Heo, M.; Kang, N.; Park, S.; Kim, J.; Hong, W. Kinetics of intermetallic compounds growth induced by electromigration of Sn-0.7Cu solder. *Korean J. Met. Mater.* **2016**, *54*, 908–915. [[CrossRef](#)]
9. Kim, B.; Lee, C.; Lee, D.; Kang, N. Effect of Sb addition on Bi-2.6Ag-0.1Cu solders for high-temperature applications. *J. Alloy Compd.* **2014**, *592*, 207–212. [[CrossRef](#)]
10. Sakai, S.; Yoshida, H.; Hiratsuka, J.; Vandecasteele, C.; Kohlmeyer, R.; Rotter, V.S.; Passarini, F.; Santini, A.; Peeler, M.; Li, J.; et al. An international comparative study of end-of-life vehicle (ELV) recycling systems. *J Mater. Cycles Waste Manag.* **2014**, *16*, 1–20. [[CrossRef](#)]
11. Dasgupta, A.; Pecht, M. Material failure mechanisms and damage models. *IEEE Trans. Reliab.* **1991**, *40*, 531–536. [[CrossRef](#)]
12. Dasgupta, A.; Hu, J.M. Failure mechanism models for plastic deformations. *IEEE Trans. Reliab.* **1992**, *41*, 168–174. [[CrossRef](#)]
13. Dieter, G.E. *Mechanical Metallurgy (Graded)*; McGraw-Hill: New York, NY, USA, 1986.
14. Coble, R.L. A model for boundary diffusion controlled creep in polycrystalline materials. *J. Appl. Phys.* **1963**, *34*, 1679–1682. [[CrossRef](#)]
15. Garofalo, F. *Fundamentals of Creep and Creep-Rupture in Metals*; McMillan Series in Material Science; McMillan: Basingstoke, UK, 1965.
16. Raj, R.; Ashby, M.F. On grain boundary sliding and diffusional creep. *Metall. Mater. Trans. B* **1971**, *2*, 1113–1127. [[CrossRef](#)]

17. Fahim, A.; Ahmed, S.; Chowdhury, M.R.; Suhling, J.C.; Lall, P. High temperature creep response of lead free solders. In Proceedings of the 15th IEEE Intersociety Conference on ITherm, Las Vegas, NV, USA, 31 May–3 June 2016; pp. 1218–1224. [CrossRef]
18. Cordova, M.E.; Shen, Y.L. Indentation versus uniaxial power-law creep: A numerical assessment. *J. Mater. Sci.* **2015**, *50*, 1394–1400. [CrossRef]
19. Hasnine, M.; Suhling, J.C.; Prorok, B.C.; Bozack, M.J.; Lall, P. Nano mechanical characterization of lead free solder joints. *MEMS Nanotechnol.* **2014**, *5*, 11–22. [CrossRef]
20. Xiag, Q.; Armstrong, W.D. Tensile creep and microstructural characterization of bulk Sn_{3.9}Ag_{0.6}Cu lead-free solder. *J. Electron. Mater.* **2005**, *34*, 196–211. [CrossRef]
21. Chen, F.; Du, Y.; Zeng, R.; Gan, G.; Du, C. Thermodynamics of oxidation on Pb-free solders at elevated temperature. *Mater. Sci. Forum* **2009**, *610–613*, 526–530. [CrossRef]
22. Ochoa, F.; Deng, X.; Chawla, N. Effects of cooling rate on creep behavior of a Sn_{3.5}Ag alloy. *J. Electron. Mater.* **2004**, *33*, 1596–1607. [CrossRef]
23. Han, I.; Eom, J.; Yun, J.; Lee, B.; Kang, C. Microstructure and hardness of 1st layer with crystallographic orientation of solidification structure in multipass weld using high Mn-Ni flux cored wire. *J. Weld. Join.* **2016**, *34*, 77–82. [CrossRef]
24. Lee, J.; Kim, H.; Lee, Y.; Choi, Y. Interfacial Properties with Kind of Surface Finish and Sn-Ag Based Lead-free Solder. *J. Weld. Join.* **2009**, *27*, 20–24. [CrossRef]
25. Park, J.; Kim, M.; Oh, C.; Do, S.; Seo, J.; Kim, D.; Hong, W. Solder joint fatigue life of flexible impact sensor module for automotive electronics. *Korean J. Met. Mater.* **2017**, *55*, 232–240. [CrossRef]
26. Seo, S.; Kang, S.; Shih, D.; Lee, H. The evolution of microstructure and microhardness of Sn-Ag and Sn-Cu solders during high temperature aging. *Microelectron. Reliab.* **2009**, *49*, 288–295. [CrossRef]
27. Hong, W.; Kim, W.; Park, N.; Kim, K. Activation energy for intermetallic compound formation of Sn-40Pb/Cu and Sn-3.0Ag-0.5Cu/Cu Solder joints. *J. Weld. Join.* **2007**, *25*, 184–190. [CrossRef]
28. Morando, C.; Fornaro, O.; Garbellini, O.; Palacio, H. Microstructure evolution during the aging at elevated temperature of Sn-Ag-Cu solder alloys. *Procedia Mater. Sci.* **2012**, *1*, 80–86. [CrossRef]
29. Kerr, M.; Chawla, N. Creep deformation behavior of Sn-3.5Ag solder/Cu couple at small length scales. *Acta Mater.* **2004**, *52*, 4527–4535. [CrossRef]
30. ISO. *ISO/TC25 Cast Irons and Pig Irons*; ISO: Geneva, Switzerland; Available online: <https://www.iso.org/committee/47206/x/catalogue/> (accessed on 3 December 2017).
31. Saganuma, K.; Huh, S.; Kim, K.; Nakase, H.; Nakamura, Y. Effect of Ag content on Properties of Sn-Ag Binary Alloy Solder. *Mater. Trans. JIM* **2001**, *42*, 286–291. [CrossRef]
32. Masayoshi, S.; Noboru, H.; Hirohiko, W.; Masayuki, Y. High Temperature Creep Properties of Sn-3.5Ag and Sn-5Sb Lead-free Solder Alloys. *Trans. JWRI* **2011**, *40*, 49–54.
33. Wang, R.; Garcia, C.I.; Hua, M.; Deardo, A. Microstructure and precipitation behavior of Nb, Ti complex Microalloyed steel produced by compact strip processing. *ISIJ Int.* **2006**, *46*, 1345–1353. [CrossRef]

